# An analytical relationship for calculating the surface evaporation rate of the $AL_2O_3$ and $TiO_2$ nanofluids using numerical and RSM methods

**Morteza Bayati** ( mbayati@uut.ac.ir )
Urmia University of Technology
**Mohsen Tahmasebi Sarvestani**
Islamic Azad University

**Research Article**

**Keywords:** surface evaporation rate, nanofluid, response surface method

**Posted Date:** March 10th, 2022

**DOI:** https://doi.org/10.21203/rs.3.rs-1404284/v1

# Abstract

The surface evaporation rate of water as a base fluid and $Al_2O_3$ and $TiO_2$ nanofluids have been investigated numerically and analytically. The numerical analysis was performed through a 3D-CFD code. The analytical study was formed by the response surface method (RSM) to optimize the old analytical relationships for pure water, including various effects affecting the evaporation rate and applying them to nanoparticles. The obtained results were validated with experimental and correlation results in the literature. The optimization process was done to obtain an algebraic expression to predict the surface evaporation rate that includes the factors affecting evaporation. Then, the RSM method got the maximum and minimum values of the evaporation rate. It was found that the presence of the nanoparticles in the base fluid leads to a change in the saturation vapor pressure and subsequently changes the surface evaporation rate of the base fluid. In this research a correlation for surface evaporation rate in terms of input parameters such as air velocity, the saturation vapor pressure of the nanofluid, relative humidity, nanofluid, air temperature, nanoparticle size, and concentration of the nanoparticle was obtained.


# 1. Introduction

The evaporation phenomenon is a process along with phase changing that has high importance in the heat and mass transfer viewpoint [1]. The mass transfer in space is equal to the mass exchanging process on the molecular scale [2]. The evaporation phenomenon is applicable in industrial environments such as cooling production, drying process, fossil fuels, combustion, etc. in natural places, undesirable evaporation from the water surface in the lake of the dams, solar pools, and farms leads to losing the water as well as the energy [3].

Nanofluids are solutions that include suspended solid nanoparticles with a size range of 10 to 100 nanometers [4–5]. They present different Thermophysical properties rather than the base fluid [6–8]. Therefore, it is expected the presence of nanoparticles in the base fluid leads to a change in the surface evaporation rate of the base fluid. The interest in this topic has led to many investigations by the researchers. Still, more researches are limited and have been done on pure water, soluble chemical materials in the water, droplets of the nanofluids. However, the need for research on the effect of different diameters and concentrations of nanoparticles on the evaporation rate is felt.

Researchers have studied the phenomenon of surface evaporation and the factors affecting it more experimentally and semi-analytically. Raimundo [9] showed that the air velocity, water-air temperature difference, and relative humidity of the air are the parameters that affect the surface evaporation rate of the water. Chu [10] studied the class A evaporation pan. They achieved that the water’s depth in the pan affected the air velocity and the evaporation rate from the water surface. The effect of the wind blow on the evaporation from the reservoir surface of the semi-Sistan reservoir was studied by Daneshkar [11] with the Dalton method. Their study showed that the primitive Dalton model is more suitable for their project. Moghiman and Joudat [12] studied the water's evaporation rate in an indoor swimming pool. They investigated the effect of the airflow passing through the water surface. An experimental study on the effect of the chemical and physical methods of reducing the surface evaporation from the water has been done by

Piri [13]. They use Cetyl and stearyl alcohols as the chemical methods and polyester as the physical method. The results that they extracted from their investigation showed that using the alcohol leads to reduce the surface evaporation rate of the water by about 40–50 percent, and the use of the polyester in the coating has a reduced effect on the surface evaporation rate of the water about 30–55 percent. Slowing down, the amount of water evaporation using the Jojoba alcohol, is one of the experimental analyses carried out by Kavianpour [14]. The obtained results showed that the effect of this alcohol on reducing the surface evaporation rate is more than Cetyl and Stril alcohols. The experimental investigation on heavier alcohols done by Piri [15] showed that Octadecanoyl alcohol has a more reduction effect on the surface evaporation rate than Hexadecanol alcohol. They also found that the correct implementation method of these alcohols can reduce the surface evaporation rate to an acceptable level. From the investigation of the insoluble nanoparticles on the droplet evaporation by Wei [16], the result showed that the value of the Pecklet number is related to the droplet's evaporation rate. Moghiman and Aslani [17] performed some experiments on several nanoparticles. Their experiment was in such a way that the surface evaporation rate of nanofluids made of these nanoparticles was obtained at the various velocity of air passing through the nanofluid surface. This study showed that the nanoparticle type could affect the evaporation rate. They also achieved that the air velocity and nanoparticle concentration directly affect reducing and increasing evaporation performance. Tso and Chao [18] studied some parameters of several nanofluids, such as the saturated vapor pressure, enthalpy of evaporation, and evaporation rate. They showed that the enthalpy of evaporation of the nanofluid reduces with an increase in the nanoparticle concentration and the highest concentration results in the lowest enthalpy of evaporation. Their study about the saturated vapor pressure and the evaporation rate of the nanofluids showed that the investigated nanofluids have lower saturated vapor pressure and evaporation rate compared with the pure water as the base fluid. Still, a few nanofluids have a higher evaporation rate and saturation vapor pressure than the water. Few researchers have worked numerically on the mass transfer of evaporation. Zhong [19] numerically studied the effect of airflow velocity and ambient humidity on the evaporation rate. Galeev [20] investigated the numerical analysis of flammable vapor cloud formation from the gasoline pool.

At present work, two type of nanofluids have been studied numerically and analytically. These are the $Al_2O_3$ and $TiO_2$ nanofluids. In the first step, the surface evaporation rate of the $Al_2O_3$ nanofluid has been investigated in three sizes and each size in three concentrations. Then, the investigation mentioned above has been done for the $TiO_2$ nanofluid in one size and three concentrations. Finally, the results were analyzed by Response Surface Method (RSM) method to optimize the old analytical relationships for pure water and include various effects affecting the rate of evaporation and applying to nanoparticles. The minimum and maximum values of the surface evaporation of the nanofluids were obtained by RSM analysis. The model described here seems to be particularly useful in studies dealing with the prediction of airflow structure, heat and mass fluxes, human thermal comfort, and energy consumption within spaces with fluid surfaces.

## 2. Numerical Solution

## 2.1. Geometrical Description

The geometry studied in this work was taken from the study of Raimundo. Figure 1 shows the schematic representation of the geometry of the evaporation tank. The computational domain has a square cross-section of 0.4 × 0.4 $m^2$ (H×W) and a length of 3.3 m (L). The maximum velocity is 0.697 m/s. The working fluid is a mixture of dry air and water vapor. The water container is a square section of 0.15 m sides, placed with its leading-edge 1.80 m from the inlet section of the domain. According to some studies [21–23], it can be assumed that the thermal radiation heat transfers between the walls and the water surface is insignificant in such present circumstances. Soret and Duffour effects between walls and the fluid surface are not considered.

# 2.2. Governing Equations

This study used the computational fluid dynamics method to solve all problem-solving processes. A 3D CFD program based on finite volume methodology was selected to run the numerical solution. The flow is incompressible, three-dimensional, turbulent, non-isothermal, mass transfer, and steady-state. The dry air and the water vapor are assumed as non-reacting independent fluids. This gaseous binary mixture behaves as a Newton-Fourier-Fick fluid. The thermophysical properties density, dynamic viscosity, thermal conductivity, and heat capacity of both fluids are taken at the local fluid moisture temperature *T* of each fluid, according to Zografos [24]. The vapor pressure is considered in constant value for the whole airflow domain. The density and the heat capacity at constant pressure obtained from Dalton's law and mole fraction of component. Equations of Butler and Brokaw [25] and Wilke [26] have been used to gain the mixture's thermal conductivity and dynamic viscosity, respectively. The binary diffusion coefficient of the water vapor into the air is suggested by Fuller [27] is used. The conservation equations are also as below. The *k* and $\varepsilon$ two-layer turbulence equation proposed by Launder and Spalding [28] is used to solve the flow turbulence.

$$\frac{\partial}{\partial_{X_i}}\left(\rho K U_i\right) = \frac{\partial}{\partial_{X_j}}\left[\left(\mu + \frac{\mu_t}{\sigma_k}\right)\frac{\partial_K}{\partial_{X_j}}\right] + G_K + G_b - \rho\epsilon$$

1

$$\frac{\partial}{\partial_{X_i}}\left(\rho \epsilon U_i\right) = \frac{\partial}{\partial_{X_j}}\left[\left(\mu + \frac{\mu_t}{\sigma_\epsilon}\right)\frac{\partial_\epsilon}{\partial_{X_j}}\right] + C_{1\epsilon}\frac{\epsilon}{K}G_K - C_{2\epsilon}\rho\frac{\epsilon^2}{K}$$

2

In which $\mu_t$ is eddy viscosity and is equal to:

$$\mu_t = \rho C_\mu \frac{K^2}{\epsilon}$$

3

And $G_K$ is turbulence kinetic energy production due to mean velocity gradient, s and it is equal to:

$$G_K = -\rho \overline{u_i' u_j'} \frac{\partial u_j}{\partial x_i}$$

4

And $G_b$ represents turbulence production due to buoyancy which is equal to:

$$G_b = \beta g_i \frac{\mu_t}{Pr_t} \frac{\partial T}{\partial X_i}$$

5

In which g indicates gravity vector in *i* direction. $Pr_t$ Indicate the turbulence Prandtl number for energy which in this case its amount is considered equal to 0.9 [29]. $\beta$ represents thermal expansion coefficient:

\beta =-\frac{1}{\rho }{\left(\frac{{\partial }_{\rho }}{{\partial }_{T}}\right)}_{P}

6

Model constants are also equal to {C}_{1\epsilon }=1.44, {C}_{2\epsilon }=1.92, {C}_{\mu }=0.09, {\sigma }_{k}=1.0 and {\sigma }_{\epsilon }=1.3.

Continuity, momentum, and energy equations are described as following. The continuity equation is equal to:

\nabla \bullet \left(\rho V\right)=0

7

The well-known momentum equation is also as below [30]:

$$\nabla \cdot (\rho V^2) = -\nabla P + \nabla \cdot (\mu \nabla V + \mu \nabla V^T) - {}^2/_3 \nabla (\mu \nabla \cdot V) + \rho g \quad (8)$$

In which *P* is static pressure and \rho g indicates gravitational body forces. The conservation of species is:

\nabla \bullet \left(\rho V{C}_{B}\right)=\nabla \bullet \left({\rho D\nabla \text{C}}_{B}\right)

9

Where *D* is the diffusion coefficient, and $C_B$ is each species' mass fraction. The energy equation is equal to:

\nabla .\left(e+\frac{{V}^{2}}{2}\right)=-\nabla \bullet \left(\rho V\right)+{W}^{\bullet }s+\rho g\bullet V-\nabla \bullet {q}^{\bullet }+\rho {q}_{\forall }^{\bullet }

10

# 2.3. Mesh independency

For analysis of grid independence in this study, the rate of mass evaporated as the base variable for comparison and imposing more refined mesh was used. Five different mesh with different sizes was compared. The grids are irregular, fine near the walls and sharp boundaries, and more nodes in the water tank. Grids with sizes of 13199, 26398, 52796, 105592, and 211184 were studied. It was observed that the change in the surface evaporation rate of water in the number of cells 105592 reaches below 1%. However,

the amount of change in the simulation results was greater as the mesh became finer. Finally, the mesh with the size of 105592 was selected for continuing the solution process.

# 3. Results

The numerical simulation of free surface evaporation of pure water is confirmed by the experimental and analytical results obtained by Raimundo and those obtained with correlations available in the literature. The evaporation rate from the water surface for pure water has been validated with the experimental and analytical results according to Eq. (11). The results of this numerical work and its differences with the experimental and analytical results are shown in Table I, where *Va* is the mean velocity of air, *Ta* is average airflow temperature, *Pa* is the partial pressure of the water vapor contained in the air, *Tw* is the water temperature at the free surface and *Pw* is the partial pressure of saturated vapor at water temperature. The achieved results from this study are in good agreement with the experimental and analytical results.

J=1\text{*}{10}^{-6}\times (37.17+32.19\text{V}\text{a})(\text{P}\text{w}-\text{P}\text{a})
11

The mass flux *J* corresponds to the evaporation rate from the corresponding surface in $grs^{-1}m^{-2}$. The subscripts *fr* refers to the formula or analytical results and *sim* to the numerical simulation.

**Table I.** numerical results and their validation with experimental and analytical results.

| Va | Ta | Tw | Pw | Pa | J-exp. | J-fr. | J-sim. | The difference with exp. | The difference with analytical. |
|---|---|---|---|---|---|---|---|---|---|
| | 293.3 | 301.9 | 3951.57 | 1900.57 | 0.059 | 0.0831 | 0.0625 | 5.9% | 24.6% |
| 0.101 | 294.6 | 307.9 | 5551.65 | 1525.65 | 0.136 | 0.1631 | 0.125 | 8.08% | 23.1% |
| | 293.9 | 315.3 | 8274.49 | 1439.49 | 0.27 | 0.2763 | 0.25 | 7.40% | 9.5% |
| | 293.1 | 317.7 | 9375.17 | 1407.17 | 0.342 | 0.322 | 0.305 | 10.8% | 5.3% |
| | 295.5 | 301.3 | 3816.25 | 1809.25 | 0.081 | 0.087 | 0.0875 | 8.02% | 0.42% |
| 0.194 | 293.6 | 309.1 | 5931.59 | 1502.59 | 0.182 | 0.192 | 0.1875 | 3.02% | 2.4% |
| | 294 | 315.2 | 8231.16 | 1445.16 | 0.287 | 0.295 | 0.275 | 4.1% | 6.6% |
| | 295 | 319 | 10022.4 | 1757.4 | 0.355 | 0.359 | 0.315 | 11.2% | 12.2% |
| | 295.1 | 301.1 | 3772.04 | 1922.04 | 0.087 | 0.087 | 0.075 | 13.7% | 13.8% |
| 0.308 | 294.9 | 309.8 | 6163.45 | 1962.45 | 0.208 | 0.198 | 0.1875 | 9.8% | 5.20% |
| | 295.4 | 314.2 | 7808.47 | 1732.47 | 0.294 | 0.286 | 0.262 | 10.8% | 8.4% |
| | 295.5 | 319.3 | 10177 | 1836 | 0.401 | 0.393 | 0.369 | 7.9% | 6.04% |
| | 295.1 | 300.8 | 3706.58 | 1730.58 | 0.106 | 0.099 | 0.093 | 12.2% | 6.3% |
| 0.406 | 295.9 | 308.2 | 5644.6 | 1503.6 | 0.206 | 0.208 | 0.2 | 2.9% | 3.8% |
| | 295.3 | 314.2 | 7808.47 | 1898.47 | 0.301 | 0.297 | 0.325 | 7.9% | 9.4% |
| | 297.5 | 319.4 | 10229.1 | 1817.1 | 0.4 | 0.423 | 0.393 | 1.75% | 7.006% |
| | 296.1 | 302.5 | 4091.05 | 1986.05 | 0.114 | 0.112 | 0.1125 | 1.3% | 0.5% |
| 0.497 | 294.9 | 309.9 | 6197.2 | 1959.2 | 0.244 | 0.225 | 0.25 | 2.4% | 10.9% |
| | 297 | 314.9 | 8102.33 | 1876.33 | 0.332 | 0.331 | 0.312 | 6.02% | 5.7% |
| | 291.6 | 319.3 | 10177 | 1772 | 0.449 | 0.447 | 0.41 | 8.6% | 8.2% |
| | 294.4 | 301.7 | 3906.01 | 1759.01 | 0.152 | 0.121 | 0.131 | 13.8% | 8.2% |
| 0.596 | 296.8 | 309.7 | 6129.85 | 1889.85 | 0.257 | 0.239 | 0.23 | 10.5% | 3.7% |
| | 294 | 313.7 | 7604.25 | 1837.25 | 0.328 | 0.325 | 0.31 | 5.4% | 4.6% |
| | 296.8 | 319.8 | 10439.4 | 1688.4 | 0.46 | 0.493 | 0.446 | 3.04% | 9.5% |
| | 296.2 | 301.5 | 3860.9 | 1801.9 | 0.145 | 0.123 | 0.13 | 10.3% | 5.9% |
| 0.697 | 295.9 | 308.7 | 5802.51 | 1936.51 | 0.239 | 0.230 | 0.243 | 1.6% | 5.4% |
| | 297.7 | 314.7 | 8017.41 | 1956.41 | 0.359 | 0.361 | 0.332 | 7.5% | 8.1% |

| Va | Ta | Tw | Pw | Pa | J-exp. | J-fr. | J-sim. | The difference with exp. | The difference with analytical. |
|---|---|---|---|---|---|---|---|---|---|
| | 296.6 | 319.1 | 10073.7 | 1778.7 | 0.471 | 0.494 | 0.446 | 5.3% | 9.7% |

In which the *J-exp*. And *J-analy*. Indicate the experimental and analytical results of the surface evaporation rate ($grs^{-1}m^{-2}$), respectively, obtained by Raimundo.

The effect of adding the $Al_2O_3$ and $TiO_2$ nanoparticles to pure water on its surface evaporation rate was investigated. In the cases of Table II, a numerical simulation process was done, and apply related nanoparticles to the pure water as the base fluid. These cases have appeared in Table II.

**Table II.** the cases that were studied for nanofluids.

| Va | Ta | Tw = Tnf | Pw | Pa |
|---|---|---|---|---|
| 0.101 | 293.9 | 315.3 | 8274.49 | 1439.49 |
| 0.194 | 294 | 315.2 | 8231.16 | 1445.16 |
| 0.308 | 295.4 | 314.2 | 7808.47 | 1732.47 |
| 0.406 | 295.3 | 314.2 | 7808.47 | 1898.47 |
| 0.497 | 297 | 314.9 | 8102.33 | 1876.33 |
| 0.596 | 294 | 313.7 | 7604.25 | 1837.25 |
| 0.697 | 297.7 | 314.7 | 8017.41 | 1956.41 |

Naturally, adding nanoparticles to the base fluid leads to a change in the thermophysical properties of the fluid, which also changes the surface evaporation rate of the base fluid. One of these properties that leads to a change in the surface evaporation rate is the saturated vapor pressure of the fluid. Table III represents the saturated vapor pressure of the nanofluids with different sizes and concentrations in all nanofluids working temperatures against that of the base fluid (pure water) for the 7 cases selected in Table II.

**Table III.** saturated vapor pressure of nanofluids with different sizes and concentrations in all working temperatures (unit: Pa)

| | Temp. (k) | 313.7 | 314.2 | 314.7 | 314.9 | 315.2 | 315.3 |
|---|---|---|---|---|---|---|---|
| Pure water | | 7604.25 | 7808.47 | 8017.41 | 8102.33 | 8231.16 | 8274 .49 |
| $Al_2O_3$ 13 nm | 0.5% | 7628.129 | 7868.063 | 8107.999 | 8203.972 | 8347.934 | 8395.92 |
| | 1% | 7535.773 | 7775.203 | 8014.633 | 8110.405 | 8254.063 | 8301.949 |
| | 2% | 7502.615 | 7742.265 | 7981.915 | 8077.775 | 8221.565 | 8269.495 |
| $Al_2O_3$ 20 nm | 0.5% | 7598.956 | 7840.46 | 8081.966 | 8178.568 | 8323.471 | 8371.771 |
| | 1% | 7568.686 | 7798.49 | 8028.296 | 8120.218 | 8258.101 | 8304.061 |
| | 2% | 7480.824 | 7717.208 | 7953.594 | 8048.148 | 8189.979 | 8237.255 |
| $Al_2O_3$ 80 nm | 0.5% | 7525.935 | 7768.33 | 8010.725 | 8107.683 | 8253.12 | 8301.598 |
| | 1% | 7444.445 | 7685.395 | 7926.345 | 8022.725 | 8167.295 | 8215.485 |
| | 2% | 7369.233 | 7606.263 | 7843.293 | 7938.105 | 8080.323 | 8127.729 |
| $TiO_2$ 21 nm | 0.5% | 7744.158 | 7994.938 | 8245.718 | 8346.03 | 8496.498 | 8546.654 |
| | 1% | 7656.768 | 7904.648 | 8152.528 | 8251.68 | 8400.408 | 8449.984 |
| | 2% | 7570.747 | 7817.517 | 8064.287 | 8162.995 | 8311.057 | 8360.411 |

After numerical investigating of mentioned cases for nanofluids, these cases were also investigated by some correlation in the literature. Both methods showed that adding the nanoparticles to the base fluids leads to the decreasing and increasing effects on the surface evaporation rate of the fluid, dependent on the size and the concentration of the nanoparticles. The results of all nanofluids with all sizes and concentrations have been presented in Fig. 2.

As shown in Fig. 2, nanofluids' amount surface evaporation rate with different sizes and concentrations has been compared with pure water in numerical and formula methods. In all cases, by increasing the concentration of the nanoparticles, the surface evaporation rate of the nanofluids takes a declining trend. The $TiO_2$ nanofluid, in most cases and concentrations, has a higher surface evaporation rate than pure water. Also, for $Al_2O_3$ nanofluid, with increasing sizes and concentrations of nanoparticles, nanofluid takes decreasing trend. In almost all cases and concentrations, 80 nanometers lower surface evaporation rate than water.

From Fig. 2, it's also clear that the $Al_2O_3$ nanofluid in the concentration of 0.5 percent and size of 13 nanometers has a higher evaporation rate than the base fluid in both numerical and formula methods. In 0.5 percent concentration and with a nanoparticle size of 20 nanometers, this nanofluid also has higher evaporation than the water. Still, it shows a less additive effect on the evaporation rate than the 13 nanometers size. When in 0.5 percent concentration, the size of the nanoparticle increases to 80 nanometers, the increasing trend of the surface evaporation rate will be changed so that in some cases, it's clear that the surface evaporation rate of the nanofluid is lower than that of the pure water.

In $Al_2O_3$ nanofluid with nanoparticle concentration of 1 percent, in size of 13 nanometers, the surface evaporation has been increased but lower than that of 0.5 percent concentration. In the concentration of 1 percent and size of 13 nanometers, some cases have a slower evaporation rate than the base fluid. This demonstrates that in the concentration of 1 percent, other governing parameters on the evaporation rate, such as air velocity, nanofluids temperature, etc., are also involved in reducing or increasing the surface evaporation rate. Increment the size to 20 and 80 nanometers indicates a more subtractive effect on the evaporation of the nanofluid. This decreasing effect is different in different cases.

The $Al_2O_3$ nanofluid with a 2 percent concentration has an evaporation rate lower than the base fluid in sizes of 13, 20, and 80 nanometers. With an increment in the size of the nanoparticle, this subtractive effect will be increased. It is concluded that in the 2 percent concentration of the nanofluid, the evaporation rate is less than that of the base fluid in all cases, therefore in high concentrations, the evaporation rate can be reduced.

For $TiO_2$ nanofluids, with looking at Fig. 2, it can be seen that in 0.5 percent concentration, the surface evaporation rate of all cases is higher than that of the base fluid, and even in this concentration, the cumulative effect on the evaporation is more than the $Al_2O_3$ nanofluid with the same concentration. With increasing the concentration of this nanofluid to 1 percent, it was observed that the $TiO_2$ nanofluid still has an accumulative effect on the surface evaporation but is lower than the 0.5 percent concentration. In the 2 percent concentration of this nanofluid, it can be seen that the increasing effect on surface evaporation is lower than the 0.5 and 1 percent concentrations, which indicates that with increasing the nanoparticle concentration, the surface evaporation takes a declining trend.

# 4. Optimization

The obtained results of the nanofluids were optimized by the response surface method (RSM). A correlation-based on all input parameters was achieved in the optimization process. The 3D Contours, the graph of the effectiveness of parameters on evaporation rate, the maximum, and minimum of evaporation rate have also been presented.

A relapse model was gotten for the surface evaporation rate of the nanofluids from the utilization of historical data design of RSM, which indorsed a moment request polynomial model to be fitted to the response data. The achieved final analytical model as far as a real factor appears in Eq. (12).

$$ {J}_{nf}=-13.8732+\left(0.0717\times {V}_{a}\right)+\left(4.7247e-5\times {P}_{nf}\right)+\left(0.0358\times {T}_{nf}\right)+\left(0.00707\times {T}_{a}\right)+\left(0.0068\times {RH}_{a}\right)+\left(1.1656e-5\times {N}_{s}\right)+\left(0.0004\times {N}_{cn}\right) \quad (12) $$

Multiple regression analysis techniques included in the historical data RSM design were hired to obtain the analytical model's coefficients. In Eq. (12), the effect of all variables on the evaporation rate, including airflow velocity, partial pressure, saturated vapor pressure, temperature, humidity, nanoparticle size, and concentration, are apparent.

The maximum difference between Eq. (12) results with numerical simulations and historical relations, at all velocities and concentrations of nanofluids, is less than 0.05 $grs^{-1}m^{-2}$.

# 4.1. Validation of the RSM model

Figure 3 demonstrates the anticipated surface evaporation rate against the actual surface evaporation rate (from analyses). The relapse line gave an adjusted R2 of 0.9076 and a predicted R2 of 0.8983. It demonstrates a moderately decent connection between the anticipated and trial estimations of the surface evaporation rate esteems. Adequate precision was another measurable parameter that was examined for the model. It quantifies the ratio of signal to noise ratio, and it is appropriate to have its incentive to be more prominent than 4. The sufficient exactness for the model in Eq. (12) was 29.7889 showing a good signal (a high value of adequate precision indicates an adequate signal).

Figure 4 is a normal plot of residuals that demonstrates the visual examination of the model. The residuals depict normal distribution because every one of the focuses pursues a straight-line curve for all intents and purposes. Likewise, the residuals demonstrate that no further improvement should be possible to the model by changing the response. Consequently, this diagram shows that the model in Eq. (12) can be viewed as the ideal model of the historical data RSM design of surface evaporation rate.

According to Figs. 5 and 6, with increasing relative humidity, surface evaporation has gotten the declining trend. But, from the middle of the relative humidity range to the end, it has taken an incremental procedure. This increasing procedure is due to increasing the air velocity in high relative humidity amounts, which indicates that the effect of the air velocity on the evaporation is more than the relative humidity of the air.

It is clear from Fig. 7 that evaporation has been gained by growing the air velocity. Enhancement of the nanofluid temperature has also caused the increment in the surface evaporation of the nanofluid. Still, in high temperatures of nanofluid, this increasing procedure is not significant, which it's due to low air velocity in the high temperature of the nanofluid. Again, it is concluded that the effect of the air velocity on the evaporation rate is more than the nanofluid temperature.

The effects of the air velocity, concentration, and size of the nanoparticles on the surface evaporation rate have been shown in Figs. 8 and 9, respectively. As Figs. 8 and 9 show that the air velocity’s effect is incremental on the evaporation of the nanofluid. The nanosize and concentration effects are diminishing but small on the surface evaporation, and these parameters have been shown more clearly in Figs. 12 and 13.

In Fig. 10, impress the surface evaporation by the air velocity and saturated vapor pressure have been demonstrated. Both of these parameters have an incremental influence on the evaporation rate.

Figure 11 indicates that the evaporation rate has increased with growing the air velocity. Still, by raising the air temperature, the evaporation rate has been gotten a declining procedure, which that is because the high air temperatures have more relative humidity in this study.

Figures 12 and 13 demonstrated that the nanosize and nano concentration influence the evaporation rate separately. It can be seen clearly that both parameters have a reducing trace on the surface evaporation rate.

Finally, the input parameters values were obtained in which the surface evaporation has the maximum and minimum amounts. Table IV represents the optimized values of the maximum and minimum surface evaporation. For this purpose, the input parameters were set in the range. The surface evaporation rate as the output parameter was also set in the maximum and then minimum state.

**Table IV.** summary of optimization of surface evaporation rate.

| Process parameter | Goal | Lower Limit | Upper Limit | Optimized Condition to maximize | Optimized Condition to minimize |
|---|---|---|---|---|---|
| velocity | In range | 0.101 | 0.697 | 0.635 | 0.502 |
| Pnf | In range | 5531.93 | 7107.15 | 7010.466 | 6661.882 |
| Tnf | In range | 313.7 | 315.3 | 315.135 | 314.502 |
| Ta | In range | 293.9 | 297.7 | 295.405 | 293.95 |
| RH | In range | 58.6184 | 74.5223 | 73.823 | 66.487 |
| nano size | In range | 13 | 80 | 46.183 | 16.612 |
| nano cn | In range | 0.5 | 2 | 0.652 | 0.668 |
| surface evaporation rate | Maximize | 0.2469 | 0.3432 | 0.3504 | - |
| surface evaporation rate | minimize | 0.2469 | 0.3432 | - | 0.2465 |

# 5. Conclusion

1. Numerical solution of the surface evaporation rate in this study and validation obtained results with experimental and formula methods in the literature showed a perfect agreement between them. Therefore, it can do such extensive and advanced problems by numerical method.

2. By checking out the surface evaporation of the water as the base fluid and the $Al_2O_3$ and $TiO_2$ nanofluids, these results achieved that adding these mentioned nanoparticles to the base fluid leads to change the evaporation rate of the base fluid. As a result, many studies can be performed on these mixture's solutions.
3. It was found that at low concentrations of $Al_2O_3$ nanofluid, the surface evaporation increases, but by growing the concentration, the evaporation of this nanofluid gets a decreasing state insofar as in 2 percent concentration, the $Al_2O_3$ nanofluid has a slower evaporation rate than the base fluid.
4. For $TiO_2$ nanofluid, the evaporation rate reduces with increasing particle concentration. Nevertheless, in most cases studied for this nanofluid, the surface evaporation is higher than the pure water even with

increasing the concentration.
5. It was also detected that, by increasing the nanoparticle size of $Al_2O_3$ in the base fluid, the evaporation rate took a declining trend even at high concentrations at large sizes. Nevertheless, its evaporation rate is less than the base fluid.
6. In the optimization process of the results, a correlation for surface evaporation rate was obtained according to all input parameters. After testing this correlation with available results achieved in this study, it was found that the mentioned correlation has a small percentage error, which indicates the correctness of the obtained equation. Therefore, it can be used widely to obtain the surface evaporation rate. The maximum and minimum of the studied nanofluids were also obtained, demonstrating the potential of different nanoparticles to change the surface evaporation rate of the base fluid in the ideal state. Therefore, these can be used in systems that work by evaporation phenomenon to improve their efficiency.

# Abbreviations

| | |
|---|---|
| *v* | Velocity (m/s) |
| *T* | Temperature (Kelvin) |
| *Pa* | The partial pressure of vapor in ambient air (Pascal) |
| *Pw* | Saturated vapor pressure of the water (Pascal) |
| *J* | Surface evaporation rate (g/cm^2) |
| *RH* | Relative humidity (%) |
| *Pnf* | Saturated vapor pressure of nanofluid (Pascal) |
| *Ns* | Nanoparticle size (nanometer) |
| *Non* | Nanofluid concentration (%) |
| ***Subscripts*** | |
| *a* | air |
| *w* | water |
| *nf* | nanofluid |
| *exp* | experiment |
| *fr* | Formula (analytical method) |
| *sim* | simulation (numerical method) |

# Declarations

### Author contributions

All authors performed the analyses, discussed the results, and reviewed the manuscript. M.B. and M.T.S. wrote the manuscript.

### Data availability

The datasets used and analysed during the current study available from the corresponding author.

### Competing interests

The authors declare no competing interests.

# References


1. Linsley, R.k. *Water-resources engineering* New York: McGraw-Hill (1979).
2. Treyball, R.E. *Mass Transfer Operation* Tokyo: McGraw Hill Inc (1990).
3. Leaney, F. & Christen, E. On-farm and community scale salt disposal basins on the Riverine Plain: Evaluating basin leakage rate, disposal capacity, and plume development. *Tech. Rep*. CRC for Catchment Hydrology (2000).
4. Chen, R.H., Phuoc, T.X. & Martello, D. Effects of nanoparticles on nanofluid droplet evaporation. Int. J. Heat Mass Transf. **53**, 3677–3682 (2010).
5. Sefiane, K. & Bennacer, R. Nanofluids droplets evaporation kinetics and wetting dynamics on rough heated substrates, Adv. Colloid Interface Sci. **147**, 263–271 (2009).
6. Wang, X., Xu, X. & Choi, S. Thermal conductivity of nanoparticle-fluid mixture. Journal of Thermophysics and Heat Transfer. **13**, 474–480 (1999).
7. Tran, X.P., Howard, B. & Chyu, M.K. Synthesis and rheological properties of cation-exchanged Laponite suspensions. Colloids Surf. A Physicochem Eng. Asp. **351**, 71–77 (2009).
8. Divsalar, A., Divsalar, H., Dods, M.N., Prosser, R.W. & Tsotsis, T.T. Field Testing of a UV Photodecomposition Reactor for Siloxane Removal from Landfill Gas. Ind. Eng. Chem. Res. **58**, 16502–16515 (2019).
9. Raimundo, A.M., Gaspar, A.R., Oliveira, A.V. & Quintela, D.A. Wind tunnel measurements and numerical simulations of water evaporation in forced convection airflow. Int. J. Therm. Sci. **86**, 28–40 (2014).
10. Chu, C.R., Li, M.H., Chen, Y.Y. & Kuo, Y.H. A wind tunnel experiment on the evaporation rate of Class A evaporation pan. J. Hydrol. **381**, 221–224 (2010).
11. Daneshkar Arasteh, P., Tajrishi, M. & Mirlatifi, M. Investigation of the effect of wind speed on evaporation from the surface of the reservoir of semi-Sistan reservoir by Dalton method. Sharif: Civ. Eng. **23**, 13–20 (2007).
12. Moghiman, M. & Joudat, A. Effect of air velocity on water evaporation rate in indoor swimming pools. Iran J. Mech. Eng. **8**, 19–30 (2007).
13. Piri, M., Hesam, M., Dehghani, A. & Meftah, H.M. Experimental study on the effect of physical and chemical approach in reducing the evaporation from water surface. J. Soil Water Conserv. **17**, 141–154

(2010).

14. Kavianpour, M., kiani, A. & Nozari, N. Reduce of water tanks evaporation rates using Jojoba Alcohol. *8th Int. Civ. Eng. Conf*. Shiraz, Iran (2010).
15. Piri, M., Hesam, M., Dehghani, A., Halaghi, M.M. & Ghazali, A.A. Determining of effect of using heavy alcohols on reduction of evaporation in water storage surface. Chem. J. Agric. Sci. Nat. Res. **16**, 284–293 (2009).
16. Wei, Y., Deng, W. & Chen, R.H. Effects of insoluble nanoparticles on nanofluid droplet evaporation. Int. J. Heat Mass Transfer. **97**, 725–734 (2016).
17. Moghiman, M. & Aslani, B. Influence of nanoparticles on reducing and enhancing evaporation mass transfer and its efficiency. Int. J. Heat Mass Transfer. **61**, 114–118 (2013b).
18. Tso, C.Y. & Chao, C.Y.H. Study of enthalpy of evaporation, saturated vapor pressure and evaporation rate of aqueous nanofluids. Int. J. Heat Mass Transfer. **84**, 931–941 (2015).
19. Zhong, J., Huang, C., Wu, D. & Lin, Z. Influence factors of the evaporation rate of a solar steam generation system: A numerical study. International Journal of Heat and Mass Transfer. **128**, 860–864 (2019).
20. Galeev, A., Chistov, Y. & Ponikarov, S. Numerical analysis of flammable vapour cloud formation from gasoline pool. Process Saf. Environ. Prot. **137**, 211–222 (2020).
21. Mezaache, E.H. & Daguenet, M. Numerical study of evaporation in laminar and turbulent regions of liquid film transfer on an inclined plate. Can. J. Chem. Eng. **78**, 994–1005 (2000).
22. Sun, H., Lauriat, G. & Nicolas, X. Natural convection and wall condensation or evaporation in humid air-filled cavities subjected to wall temperature variations. Int. J. Therm. Sci. **50**, 663–679 (2011).
23. Costa, V.A.F. Transient natural convection in enclosures filled with humid air, including wall evaporation and condensation. Int. J. Heat Mass Transfer. **55**, 5479–5494 (2012).
24. Zografos, A.I., Martin, W.A. & Sunderland, J.E. Equations of properties as a function of temperature for seven fluids. Comput. Methods Appl. Mech. Eng. **61**, 177–187 (1987).
25. Butler, J.N. & Brokaw, R.S. Thermal conductivity of gas mixtures in chemical equilibrium. J. Chem. Phys. **26**, 1005–1006 (1957).
26. Wilke, C.R. A viscosity equation for gas mixtures. J. Chem. Phys. **18**, 517–519 (1950).
27. Fuller E.N., Schettler, P.D. & Giddings, J.C. New method for prediction of binary gas-phase diffusion coefficients. Ind. Eng. Chem. **58**, 18–27 (1966).
28. Launder, B.E. & Spalding, D.B. *Mathematical models of turbulence*. Academic press (1972).
29. Tominaga, Y. & Stathopoulos, T. Turbulent Schmidt numbers for CFD analysis with various types of flowfield. Atmos. Environ. **41**, 8091–8099 (2007).
30. Batchelor, G.K. *An introduction to fluid dynamics*, Cambridge university press (2000).

# Figures

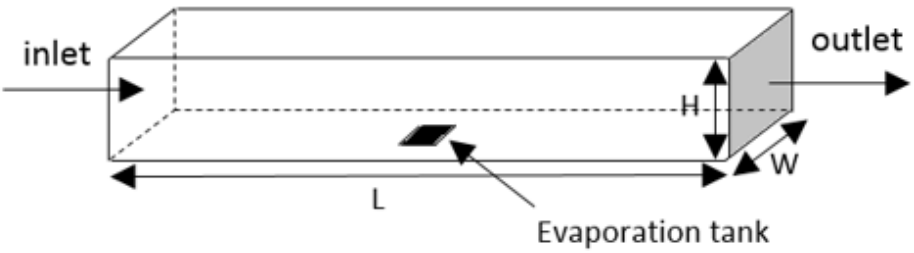


**Figure 1**

Schematic representation of the geometry.

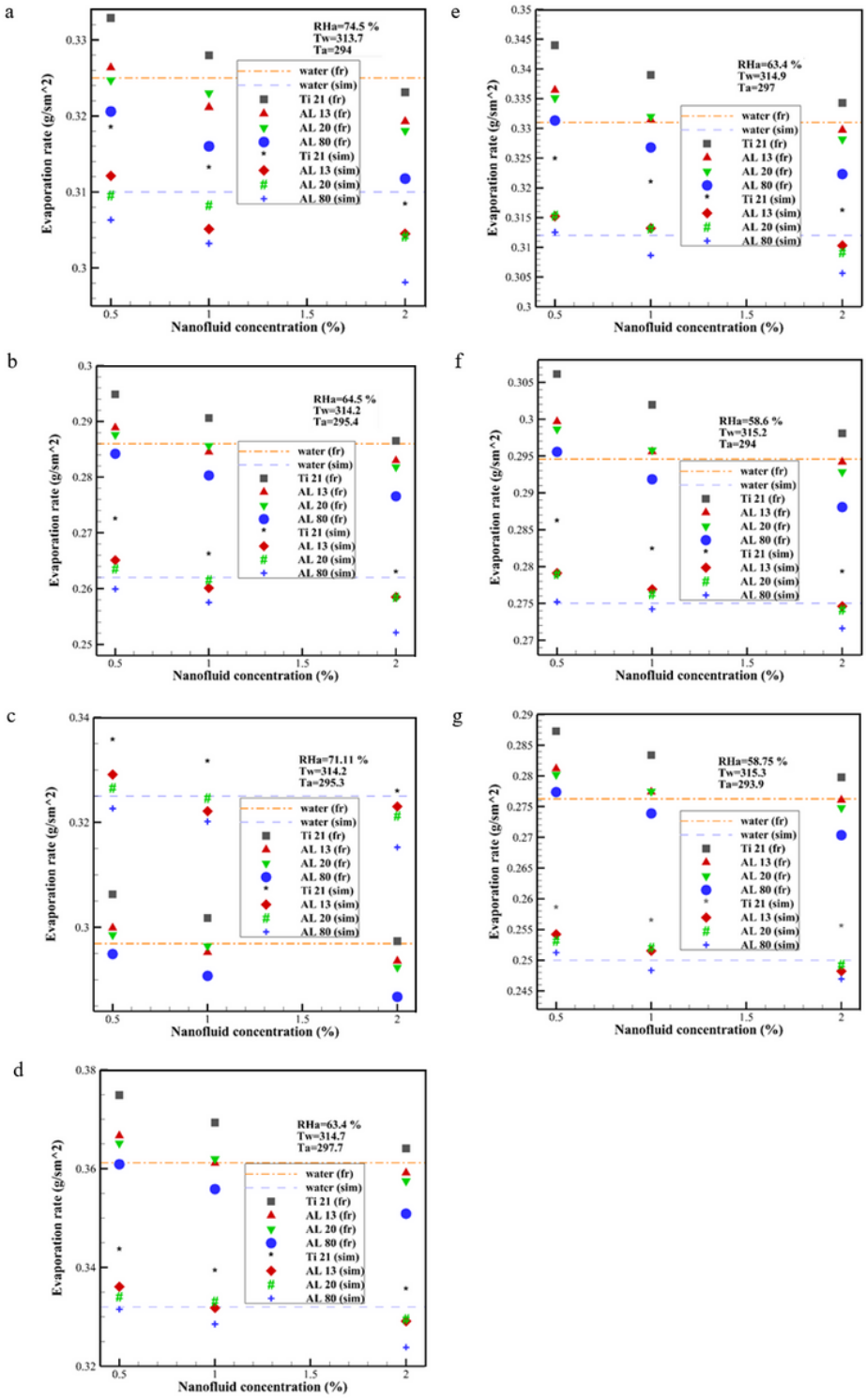


## Figure 2

surface evaporation rate of nanofluids with a: RHa=74.5 %, Tw=313.7 K, and Ta=294 K, b: RHa=64.5 %, Tw=314.2 K, and Ta=295.4 K, c: RHa=71.11%, Tw=314.2 K, and Ta=295.3 K, d: RHa=63.4%, Tw=314.7 K, and Ta=297.7 K, e: RHa=63.4%, Tw=314.9 K, and Ta=297 K, f: RHa=58.6%, Tw=315.2 K, and Ta=294 K, g: RHa=58.75%, Tw=315.3 K, and Ta= 293.9 K.

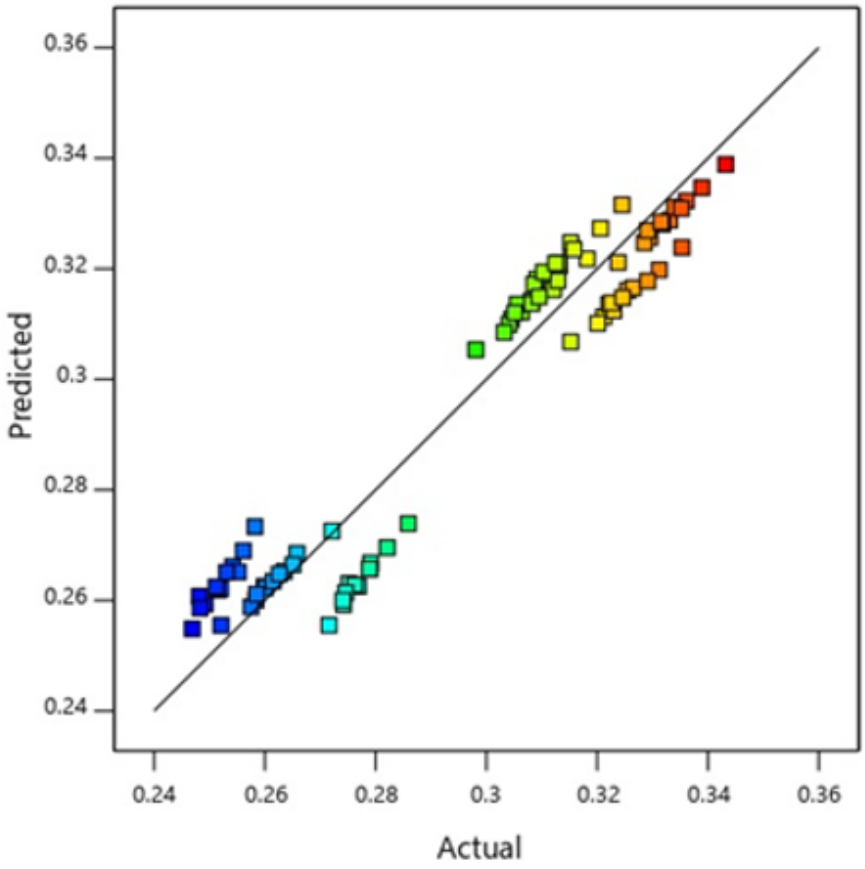


## Figure 3

Graphical representation of actual and predicted values.

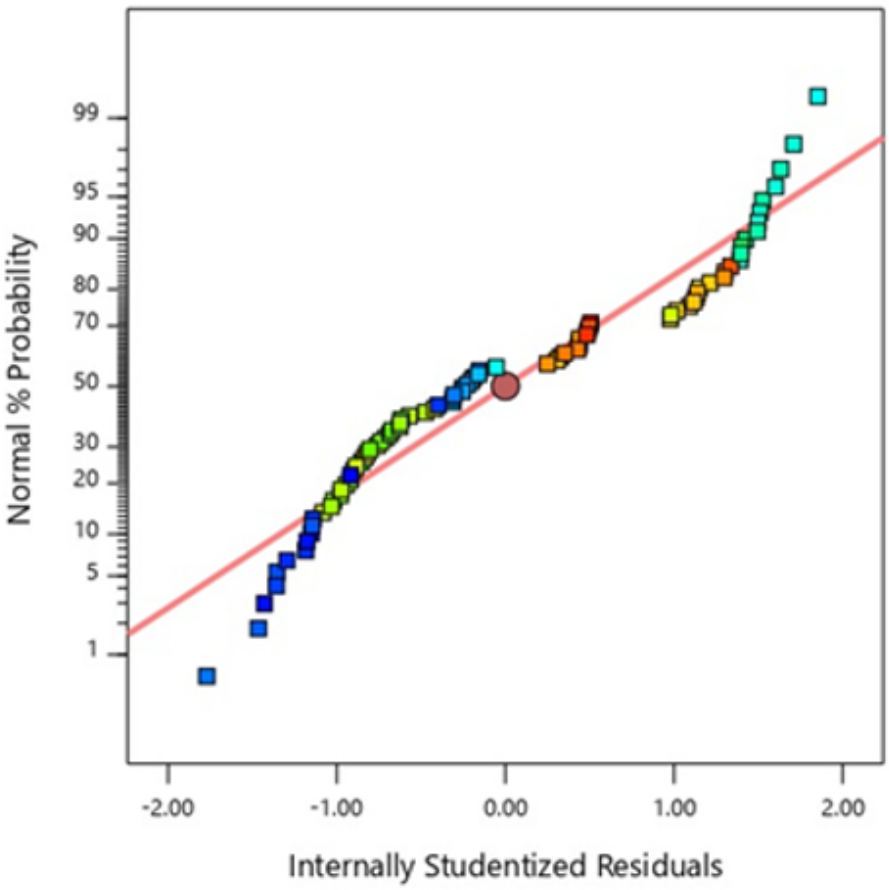


## Figure 4

Graphical representation of residuals for the model.

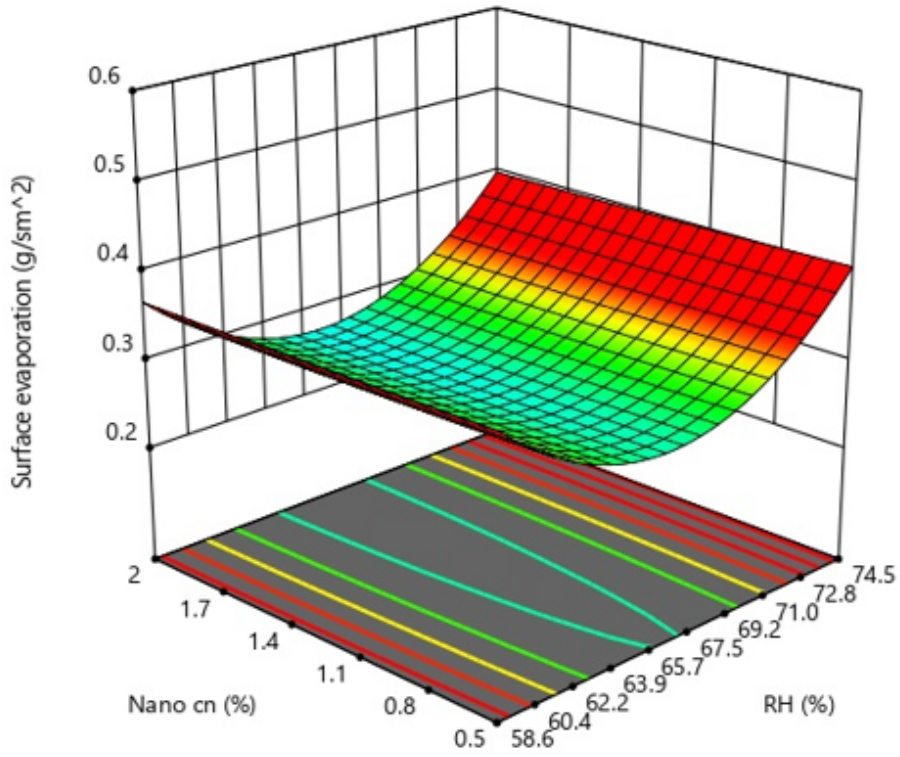

## Figure 5

3D response surface plot of nano concentration and RHa.

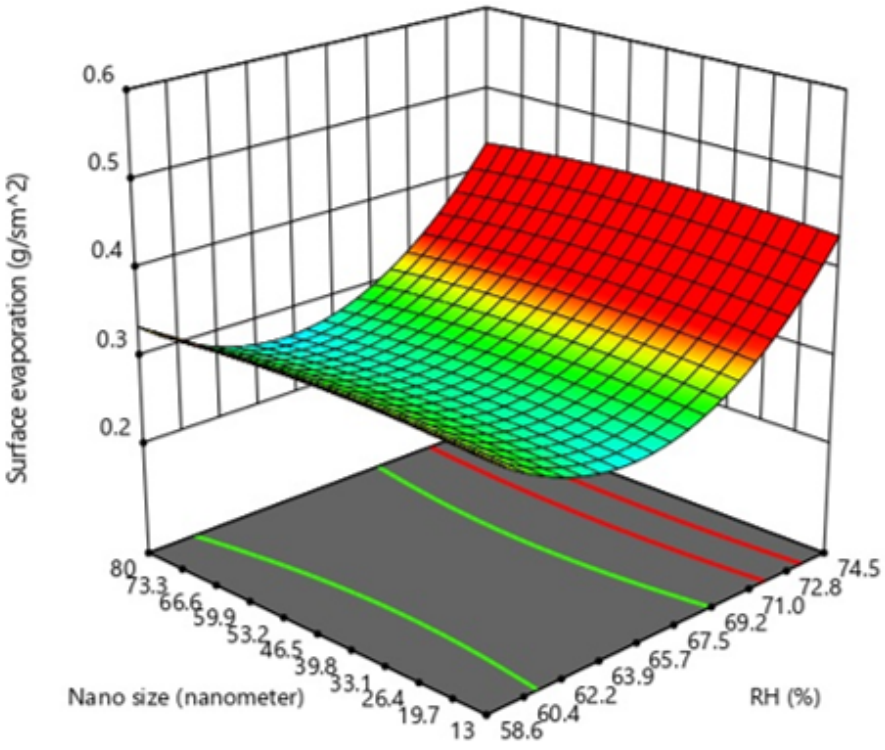


## Figure 6

3D response surface plot of nano size and RHa

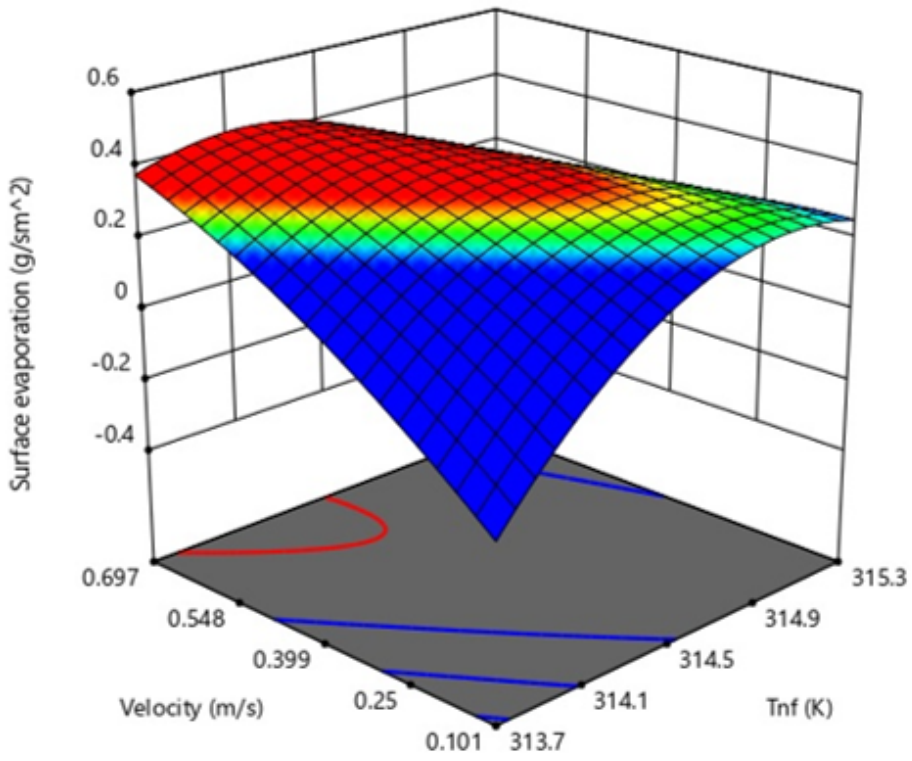


## Figure 7

3D response surface plot of air velocity and nanofluid temperature.

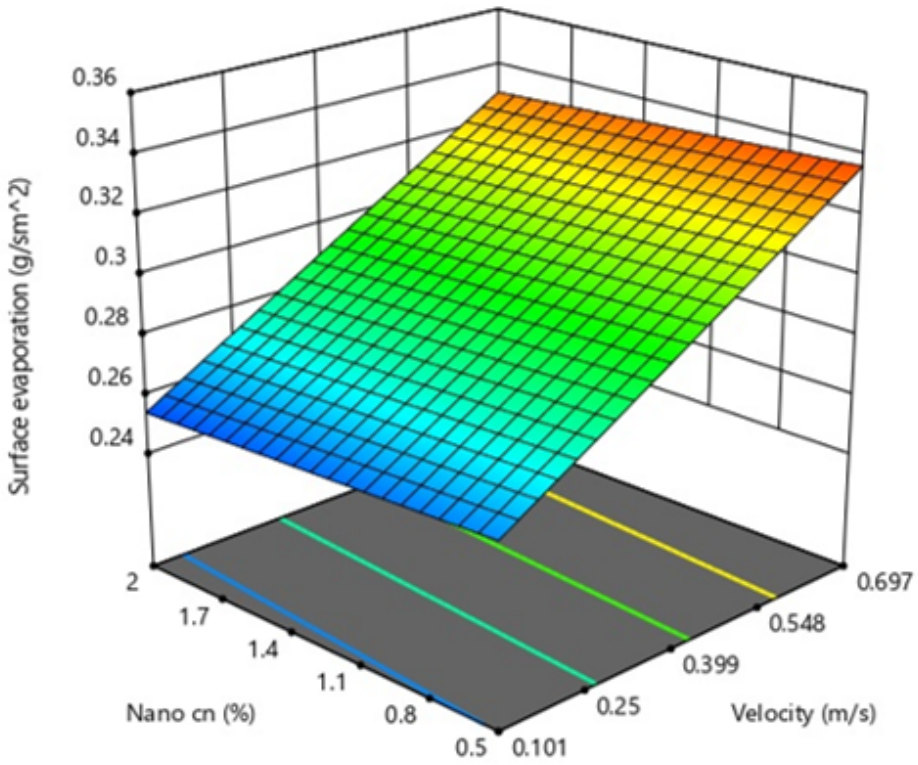


## Figure 8

3D response surface plot of nano concentration and air velocity

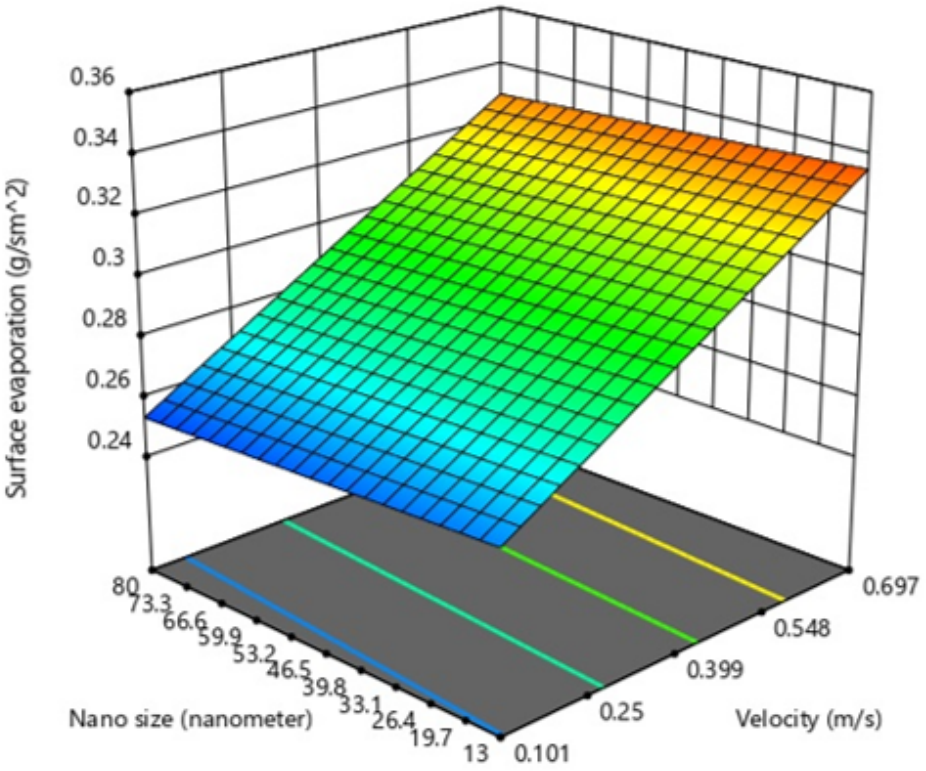


**Figure 9**

3D response surface plot of nano size and air velocity.

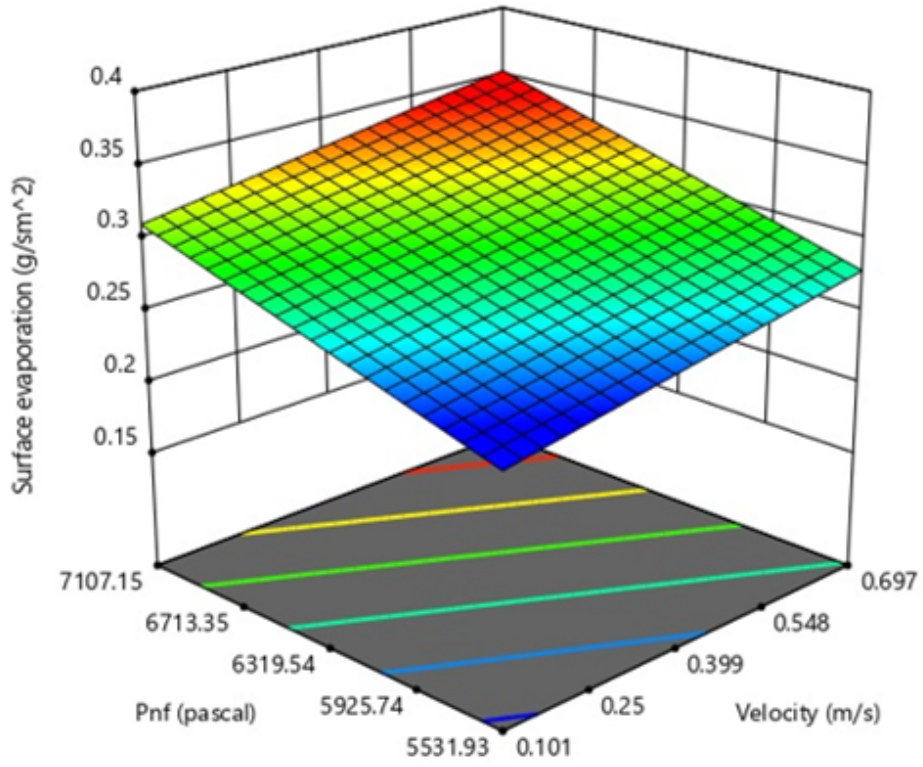

## Figure 10

3D response surface plot of the saturated vapor pressure of nanofluid and air velocity.

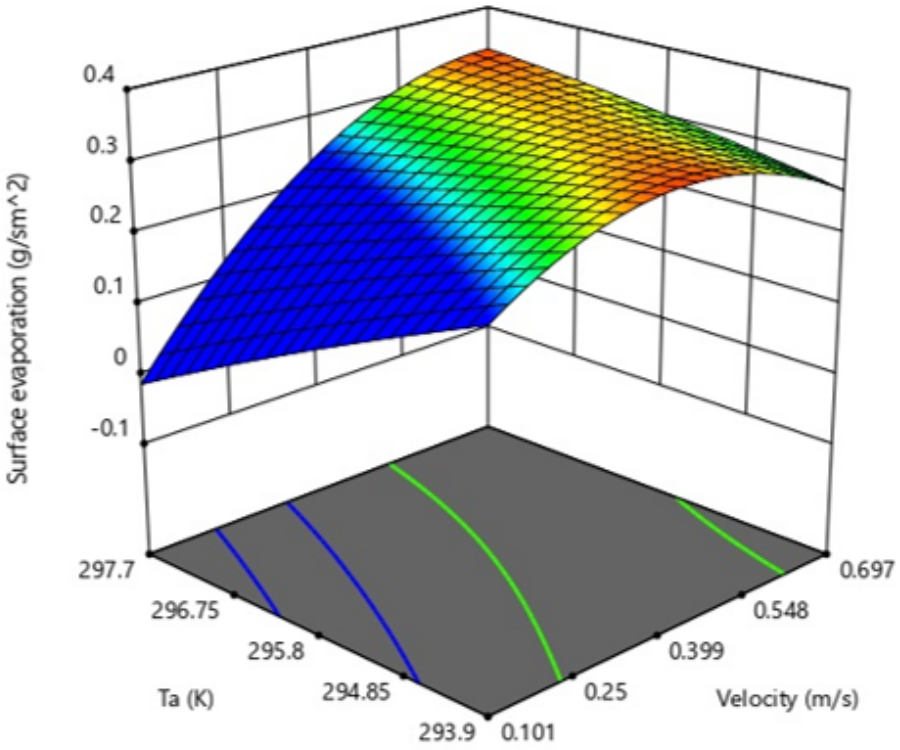


## Figure 11

3D response surface plot of air temperature and air velocity.

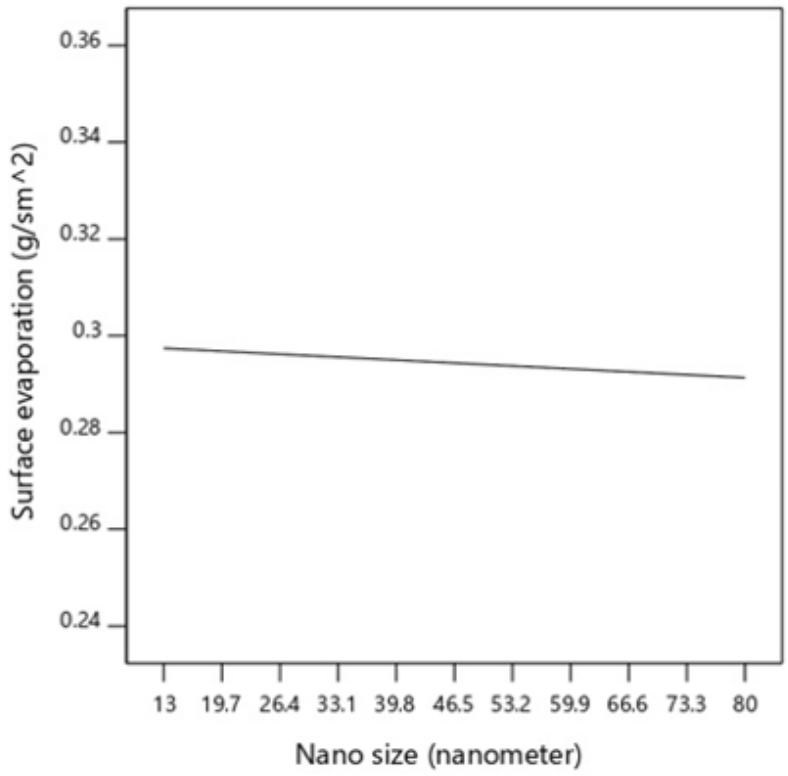


Figure 12

one-factor plot of nano size.

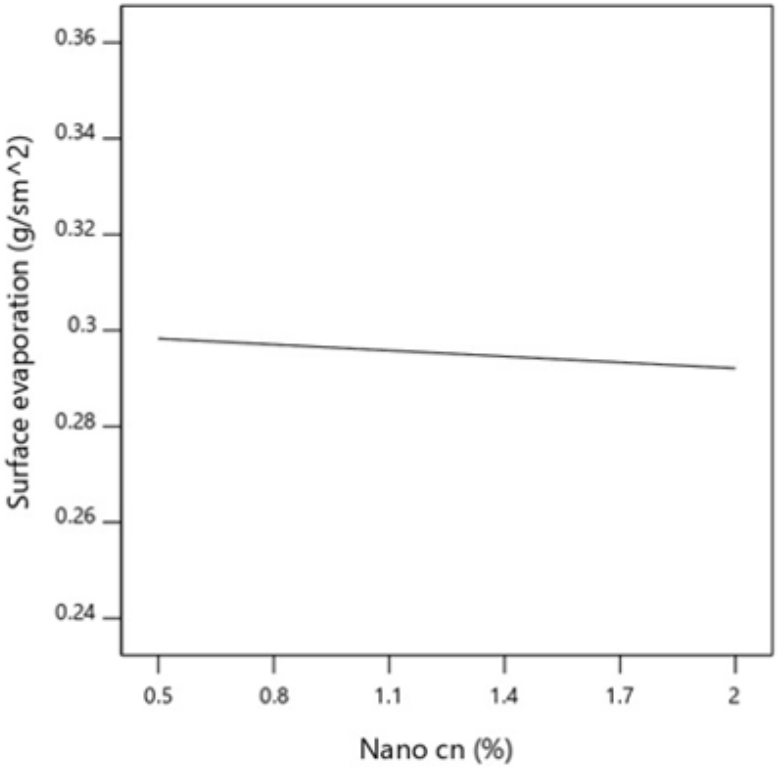


Figure 13

one-factor plot of nano concentration.